QED of strong fields: Status and recent developments

Thomas Beier, Mark Beinker, Emil Persson, Sven Zschocke and Gerhard Soff

Institut für Theoretische Physik, Technische Universität Dresden, Mommsenstr. 13,
D-01062 Dresden, Germany
E-mail: beier@physik.tu-dresden.de

We discuss the status and open problems of recent calculations on QED effects in heavy few-electron ions. In particular, we examine corrections in these systems which are not of quantum electrodynamical origin but which might influence energy shifts on the same order-of-magnitude as the accuracy of present-day QED calculations.

Keywords: Lamb shift, hydrogenlike high-Z systems, QED, g-factor

1.   Introduction

The experimental tests and also the theoretical predictions of quantum electrodynamical (QED) effects in physics belong to the most stimulating fields in science. Up to now there is no deviation from known QED results, neither for weak nor for strong electromagnetic fields. Although there is no indication that this will change in the near future, during the last years a number of highly subtile setups have been constructed to measure QED effects particularly in strong electromagnetic fields of heavy nuclei. These strong fields provide the unique opportunity to test the validity of QED in a regime where ordinary perturbation theory is no longer a suitable tool when considering the external field. Furthermore, the highly relativistic bound states in heavy hydrogenlike ions are strongly localized and, therefore, bear very high momentum components. These states also have to be investigated very carefully in the context with the search for spontaneous positron emission [1] in critical fields.

High-precision Lamb shift measurements have been performed for a number of hydrogenlike systems [2–4] as well as for some lithiumlike systems [5], where experimental precision is even higher. Also hyperfine structure measurements on several heavy few-electron high-Z systems have been carried out with a precision sufficient to probe QED predictions [6–9]. For the g-factor measurement of bound electrons in the high-Z region, only plans exist up to now, but the setup of the final experiments is developing in a promising way [10].

The corresponding theoretical evaluations try to keep ahead of the experiments but are still limited for several reasons as we are going to indicate in the following. We will focus on the Lamb shift and on the g-factor of bound electrons. The hyperfine structure is discussed elsewhere in this volume [11].

2.   Lamb shift calculations

The term "Lamb shift" is due to the famous measurement of Lamb and Retherford in 1947 [12], in which an energy difference between the $2s_{1/2}$ and the $2p_{1/2}$ state of hydrogen was observed. Relativistic Dirac theory predicted them to have exactly the same energy. The shift of the $2s_{1/2}$ state was found to be due to QED effects. Nowadays, the sum of all deviations from the point nucleus Dirac energy value for a particular state is termed Lamb shift of this state (figure 1) except for a reduced-mass correction which for historical reasons is omitted in this sum but should not be separated at all [13].

In figure 2 we display the major contributions to the Lamb shift. The QED effects self energy and vacuum polarization of order α (figure 3) yield the dominant part especially for low-Z atoms. For higher Z, also the finite extension of the nucleus has to be considered. It simply alters the pure $1/r$ Coulomb potential which is employed in the Dirac energy eigenvalue [14]. Therefore, also wave functions and energy eigenvalues change slightly. As the expectation value $\langle r \rangle$ approximately scales as $\sqrt{1 - (Z\alpha)^2}/Z$, this contribution becomes important especially for high-Z hydrogenlike systems.

All of these effects can be calculated with a relative precision of at least 10^{-5}–10^{-6} nowadays. For the QED effects, proper numerical methods were developed which are able to use the propagator of a *bound* electron in the calculations. This propagator obeys the equation

$$\left[\gamma^\mu \big(i\partial_\mu - e\, A_\mu(x_1) \big) - m_{\mathrm{e}} \right] S_F(x_1, x_2) = \delta^4(x_1 - x_2). \tag{1}$$
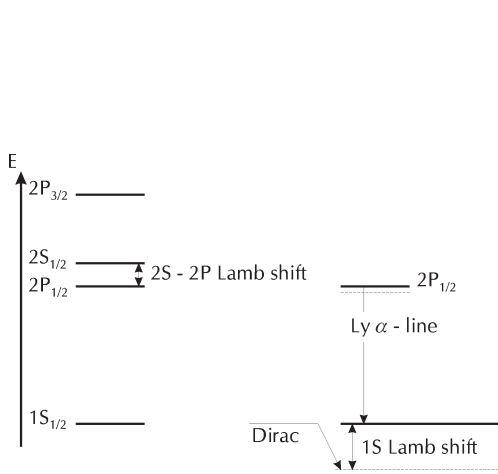
Figure 1. The energy level shifts which are subsumed as "Lamb shift".
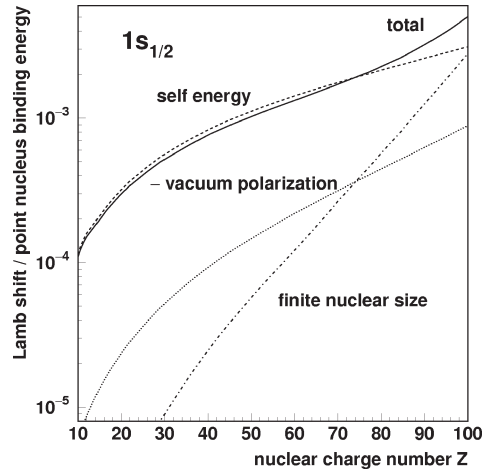
Figure 2. The $1s_{1/2}$ Lamb shift and its dominant contributions in relation to the binding energy.

The propagator can be expressed in terms of an eigenfunction expansion

$$S_F(x_1, x_2) = \Theta(t_2 - t_1) \sum_{n+} \Phi_n(x_2)\overline{\Phi}_n(x_1) - \Theta(t_1 - t_2) \sum_{n-} \Phi_n(x_2)\overline{\Phi}_n(x_1), \quad (2)$$

where the sum runs over states of positive and negative energy eigenvalues separately. In eq. (1), A_μ represents the external potential.

Employing this propagator results in a nonperturbative treatment of the external potential of the nucleus. An expansion in powers of $(Z\alpha)$ is not adopted, except in calculations for the Lamb shift in hydrogen. This advantage has its price: the use of the analytically much simpler free electron propagator is not possible, and the handling of the bound electron propagator requires a proper grouping of renormalization terms [15] as well as elaborated methods in dealing with angular momenta, such as the partial wave expansion [16]. For details we refer to original papers and to the more elaborated recent review [13].

Except for hydrogen, these three contributions are sufficient to explain all Lamb shifts measured up to now. Figure 4 displays the current level of experimental data and theoretical predictions. However, with increasing experimental precision effects may become visible that are beyond those mentioned so far.

First of all, we refer to the QED effects of second order in α. The expansion in α indicates the number of *internal* photon lines and is not to be mixed up with the $(Z\alpha)$ expansion mentioned above. The significance of a diagram may well be estimated by the number of internal photon lines (and thus powers of α) also for heavy nuclei. For $Z = 90$, the effects of the diagrams are about 1 eV, which has to be compared to about 300 eV for the self energy and 80 eV for the vacuum polarization of order α.
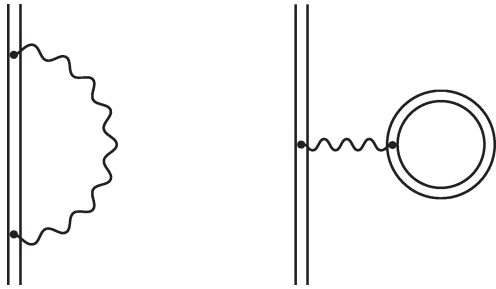
Figure 3. Self energy (left) and vacuum polarization (right) of order α, displayed as Feynman diagrams. Double lines denote bound fermion propagators, wavy lines denote photons.
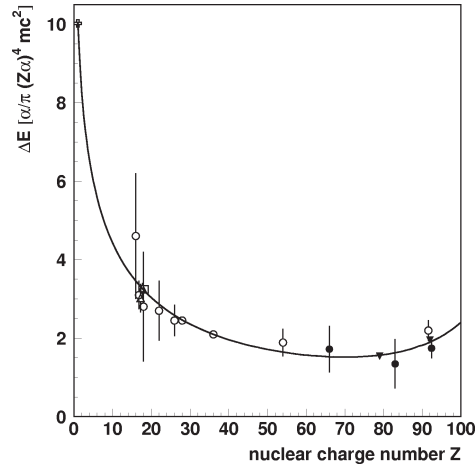
Figure 4. Experimental values and theoretical prediction for the Lamb shift of the $1s_{1/2}$ state. The diagram is normalized according to the dominant factor $(\alpha/\pi)(Z\alpha)^4 m_e c^2$.

Table 1
One-electron Lamb shift contributions for ^{232}Th. Values are given in eV.

State	$1s_{1/2}$	$2s_{1/2}$	$2p_{1/2}$
Binding energy E_B (point nucleus)	-125655.61	-32443.85	-32443.85
Correction:			
Finite nuclear size	160.52	29.92	3.29
Self energy (order α)	325.02	59.14	8.04
Vacuum polarization (order α)	-78.60	-13.65	-2.23
SESE a) b) c)		yet uncalculated	
VPVP a)	-0.18	-0.03	0.00
VPVP b)	-0.13	-0.03	0.00
VPVP c)	-0.54	-0.09	-0.02
SEVP a) b) c)	0.98	0.18	0.02
S(VP)E	0.11	0.02	0.00
Recoil	0.47	0.12	0.08
Nuclear polarization	-0.13	-0.02	0.00
Sum of corrections	407.52	75.56	9.18
Resulting total binding energy	-125248.09	-32368.29	-32434.67
Reduced mass	0.30	0.08	0.08
Lamb shift (theory)	407.22	75.48	9.10

In table 1 we display a summary of all contributions for Th. A similar table was published earlier for uranium [17].

The ten Feynman diagrams which represent QED corrections of order α^2 are displayed in figure 5, where also the current status of their evaluation is indicated. The three two-photon self-energy diagrams SESE a)–c) up to now have been analyzed only partially, although several research groups work on tackling the divergencies with promising effort ([18–20] and references therein). For the VPVP diagrams of the second row, considerable progress was made in the last year by evaluating the VPVP b) diagram to all orders by Plunien et al. [21]. The VPVP c) diagram is likely to be handled somewhat similarly, but calculations to all orders in $(Z\alpha)$ of the loop are not yet completed. The same holds true for the S(VP)E diagram in the last row [17,22]. Contrary to the failure of an expansion into powers of $(Z\alpha)$ for self-energy corrections, this expansion is still suitable for the loops in vacuum polarization diagrams. Employing propagators of free electrons in these loops leads to the Uehling contribution in vacuum polarization, where only one interaction of the loop with the external field is considered. Even for $Z = 92$, higher order terms do not contribute to more than 10% of its total vacuum polarization correction. A more detailed discussion on this can be found in [13]. For evaluation techniques of the other diagrams we refer to the original articles, namely [23,24] for VPVP a), [25,26] for VPVP c), and [17,27] for SEVP a)–c).

Beneath the pure QED effects, also a few more contributions caused by properties of the nucleus enter the Lamb shift at the same level of accuracy. These are the finite mass of the nucleus, the uncertainty in the already mentioned nuclear size and also
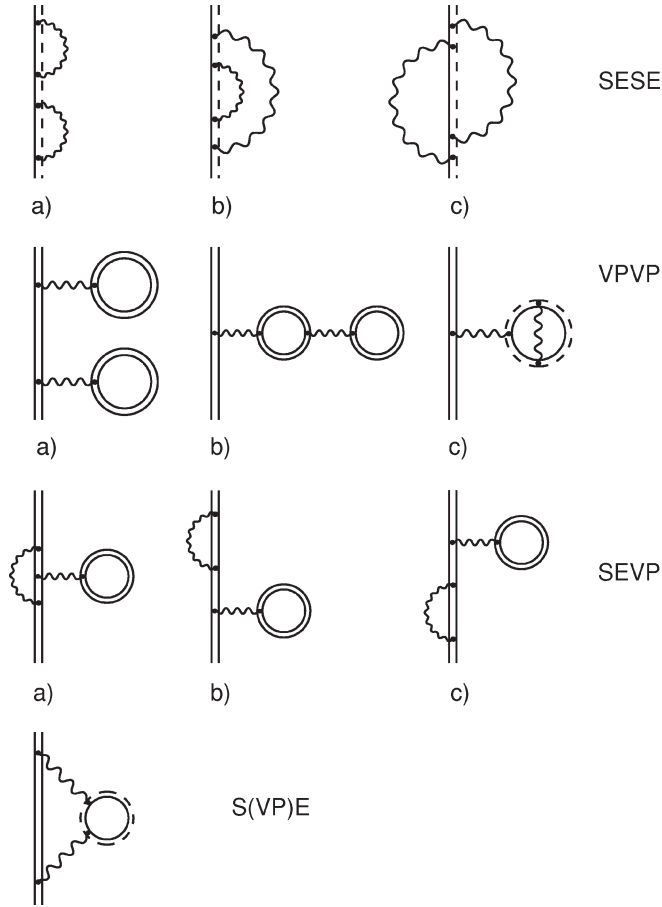
Figure 5. QED contributions of order α^2 to the Lamb shift in hydrogen-like ions. The current status of evaluation is indicated by the fermion lines. A dashed together with a solid line indicates that for this line a complete calculation was performed only with free electron propagators up to now. The letters correspond to the naming scheme of the tables.

the internal structure of the nucleus which allows for virtual excitations similar to self energy and vacuum polarization in QED.

In straightforward Dirac theory, the nucleus is considered as infinitely heavy, thus requiring no separation of any problem into relative and center-of-mass variables. Unlike in nonrelativistic theory, where this separation is sufficient, the finite speed of light causes retardation effects. The recoil effect for the Lamb shift was calculated to all orders in $(Z\alpha)$ by Artemyev et al. [28,29]. Errors due to a nonrelativistic approximative treatment of the nuclear motion are thought to be negligible compared to other sources of uncertainties.

We stress that the approach of Shabaev does not distinct between any relativistic additions and the "reduced mass" effect which results from the separation into center-of-mass and relative variables in nonrelativistic theory only and simply leads to an

energy shift of

$$\Delta E_{\text{reduced mass}\,nlj} = -\frac{m_\text{e}}{m_\text{e} + M_\text{N}} E_{nlj}, \tag{3}$$

where $E_{nlj} < 0$ denotes the binding energy, and m_e and M_N are the masses of electron and nucleus, respectively. This effect does not contribute to the classical Lamb shift between the $2\text{s}_{1/2}$ and the $2\text{p}_{1/2}$ states. For historical reasons, it is therefore *not* included in the Lamb shift of a single state, although in a fully relativistic treatment this is by no means justified. Anyhow, we present the "Sum of corrections" and the "classical" Lamb shift separately in table 1.

On the same scale as the nuclear recoil correction uncertainties caused by the nuclear size and shape also enter the predictions. All calculations are carried out for spherically symmetric nuclei. This is well justified, since deformations of the nuclei do not affect the center of a particular state (although it may split up by electrical hyperfine splitting even if $I = 0$). However, the radial nuclear charge distribution $\rho(r)$ determines the radial potential, and some differences in the energy eigenvalue are visible for different charge distributions, even if the same rms-radius $\langle r^2 \rangle^{1/2}$ is taken, which is defined as

$$\langle r^2 \rangle = \int r^4 \rho(r)\, \mathrm{d}r \Big/ \int r^2 \rho(r)\, \mathrm{d}r. \tag{4}$$

The rms-radius is widely used when comparing the influence of different nuclear models to the binding of the electrons. It is possible, however, to include higher moments of the charge distribution as well [30].

For extended nuclear charge distributions, a number of models are employed. The simpler one is the charged shell model, where the charge of the nucleus is considered to be located on a shell with radius $R = \langle r^2 \rangle^{1/2}$,

$$\rho(r) = \frac{Ze}{4\pi R^2} \delta(R - r). \tag{5}$$

More realistic, but still simple enough is the assumption of a uniform charge distribution throughout the whole nuclear extension,

$$\rho(r) = \frac{Ze}{(4/3)\pi R^3} \Theta(R - r), \tag{6}$$

where $R = \sqrt{5/3}\,\langle r^2 \rangle^{1/2}$. More elaborated is the Fermi distribution which exists in different forms [31]. Its two-parameter form reads

$$\rho(r) = Ze \frac{N}{1 + \exp\{(r - c)/a\}}, \tag{7}$$

where c denotes the half-density radius and a is a measure for the skin thickness. N is a properly chosen normalization constant.

For gold, thorium, and uranium, we indicate the effects caused by two realistic charge distributions in table 2. The difference in binding energies can be considered

Table 2
Nuclear charge distribution parameters and resulting binding energies for the $1s_{1/2}$ states in different hydrogenlike ions.

	^{197}Au^{78+}		^{232}Th^{89+}		^{238}U^{91+}	
$\langle r^2 \rangle^{1/2}$	5.437	fm	5.802	fm	5.860	fm
	± 0.011	fm	± 0.004	fm	± 0.002	fm
a	0.535	fm	0.5110	fm	0.5046	fm
$E_{\rm B}$ (Fermi distrib.)	-93410.76	eV	-125495.09	eV	-132081.14	eV
$E_{\rm B}$ (Hom. sphere)	-93410.67	eV	-125494.79	eV	-132080.78	eV
Difference	0.09	eV	0.30	eV	0.36	eV
Size uncertainty	0.16	eV	0.16	eV	0.10	eV

as an upper limit to the "shape uncertainty", whereas the "size uncertainty" merely accounts for the error in $\langle r^2 \rangle^{1/2}$ indicated in the table. Sometimes experimental measurements appear with a new value for the nuclear radius which lies well outside the error limits of an old one. For details of experimental procedures in defining nuclear size and shape we refer to [31,32].

The QED effects of order α are also influenced by the nuclear size in a way which is visible in precise calculations. Employing the propagator of a bound electron implies the utilization of the proper potential in (1). Different nuclear sizes and shapes cause different potentials and thus slightly different electron propagators. The shape does not affect the numerical values considerably if the same rms-radius is employed [33]. If nuclei of different size are considered, the effect is well above the numerical precision. We demonstrate this for ^{232}Th, where the published radius changed considerably within the last twenty years. It was reported to be $\langle r^2 \rangle^{1/2} = 5.707$ fm [34], but a newer measurement of Zumbro et al. [35] resulted in $\langle r^2 \rangle^{1/2} = 5.802$ fm. In table 3 we display finite size effects and QED contributions of order α calculated with both nuclear radii. The main contribution to the difference results from the size effect itself, but the change in size is also noticeable for each of the QED contributions separately. Only when added together it becomes one order smaller in magnitude.

Not discussed so far are effects due to the internal structure of the nucleus. Classically speaking, we can think of vacuum polarization as an excitation of virtual electron–positron pairs by exchanging photons with the propagating electron. The same can be imagined for the nucleus. As it possesses internal structure, it can also be virtually excited by coupling to the electron. This is termed nuclear polarization. For the Lamb shift in highly charged ions, this was elaborately evaluated by Plunien et al. [36]. We are not going to discuss this effect here in detail but refer to the original articles and to the overview presented in [13]. For the purpose of this work it should be noted that the nuclear states and parameters that enter the nuclear polarization calculation, are known from experiment only and are not very precise sometimes. This is the limit to the accuracy of nuclear polarization calculations which is thought to be precise only to about 20% of its value.

Table 3
Main contributions to the Lamb shift in ^{232}Th^{89+} for different nuclear radii. Values
are given in eV.

Contribution	$\langle r^2 \rangle^{1/2} = 5.802$ fm	$\langle r^2 \rangle^{1/2} = 5.707$ fm	Difference
	$1s_{1/2}$ state		
Finite size	160.52	156.59	3.93
Self energy	325.02	325.09	−0.07
Vacuum polarization	−78.60	−78.65	0.05
Total QED (order α)	246.42	246.44	−0.02
Total	406.94	403.03	3.91
	$2s_{1/2}$ state		
Finite size	29.92	29.19	0.73
Self energy	59.14	59.16	−0.02
Vacuum polarization	−13.65	−13.66	0.01
Total QED (order α)	45.49	45.50	−0.01
Total	75.41	74.69	0.72
	$2p_{1/2}$ state		
Finite size	3.29	3.21	0.08
Self energy	8.04	8.04	0.00
Vacuum polarization	−2.23	−2.23	0.00
Total QED (order α)	5.81	5.81	0.00
Total	9.10	9.02	0.08

The level schemes which are employed in the calculations are based on nuclear models and do not account for the quark structure of hadronic matter. This, however, does not result in a large uncertainty alltogether since the description of the nucleus in these model schemes is quite elaborate and reliable for our purposes. Anyhow, the nuclear polarization determines the final limit to any QED predictions in heavy hydrogenlike ions, since for deviations between theory and experiment on this level of magnitude it would not be clear whether they are due to insufficiently known nuclear structure effects or simply due to deviations of QED theory from real nature.

Another effect which we will mention here only is the exchange of a boson different from a photon. In electroweak interaction, the exchange of a Z_0 boson is also possible without any transfer of charge. This process normally is separated into a "parity conserving" part and a "parity violating" part, where this terminology refers to the occurrence of transitions which are allowed or forbidden, respectively, by selection rules of pure photon exchange. The parity violating part is important for lifetime considerations of atomic levels which we are not discussing here.

The parity conserving part, however, gives also rise to a small energy shift which reads [37]

$$\Delta E_{\mathrm{W}} = \langle H_{\mathrm{W}} \rangle, \qquad (8)$$

where the subscript W denotes "weak interaction". The Hamiltonian of (8) reads (in natural units)

$$H_{\mathrm{W}} = \frac{G}{2\sqrt{2}} \big[N(1 - 4\xi) - Z(1 - 4\xi)^2 \big] \delta(\mathbf{r}). \qquad (9)$$

Here, $G \simeq 10^{-5}\, m_{\mathrm{p}}^{-2}$ is the Fermi coupling constant, which is expressed by the proton mass m_{p}. N and Z denote number of neutrons and protons in the system under consideration, and $\xi = \sin^2 \Theta_{\mathrm{W}} \simeq 0.23$ is connected to the Weinberg angle Θ_{W}, which relates the couplings in electroweak interaction.

For the $1\mathrm{s}_{1/2}$ state of U^{91+}, the associated energy shift was calculated to be 0.59×10^{-5} eV [37]. By this it is clear, that any effect caused by weak interaction is not likely to be visible in any Lamb shift measurement of hydrogenlike ions at all.

Another effect which has not been considered up to now with sufficient accuracy is the effect of boundaries. Any spectroscopic measurement takes place in a physical chamber and (except for some trap measurements) also in the company of other particles in the beam. These boundaries impose themselves an influence to radiative corrections. The most prominent of the features caused by this is the attraction of two neutral perfectly conducting plates in the vacuum [38]. This effect has been verified experimentally and is named Casimir effect after its discoverer. For an overview, we refer to [39]. We stress that there are no proper investigations on the actual size of boundary effects in heavy hydrogenlike ions up to now.

So far we have considered only hydrogenlike ions. To our opinion, they represent the simplest and also most beautiful system for investigating effects of strong electromagnetic fields. However, also heliumlike and lithiumlike ions have been investigated both by experiment and theory, and the experimental results are even more precise than in the one-electron case. For uranium, we display the current theoretical predictions in table 4. This table is a slightly modified version of the one published in [17] due to some improved calculations. For details we refer to [17].

This table displays some drawbacks. First, the energy eigenvalues and the electron wave functions can be computed numerically from the beginning only – in contradiction to the one-electron case, where at least for the point nucleus an analytical solution exists which can serve as a starting point. The electron–electron interaction effects are contained in the "RMBPT" entry.

Second, due to the photon exchange between the electrons some more interactions come into play, which also have to be corrected for QED contributions (screening effects). Another effect is the exchange of more than one photon between the electrons (two-photon entries). In summary, theory is well in agreement with experiment.

Table 4
$2p_{1/2}$–$2s_{1/2}$ shift in Li-like U. The total theoretical error arises from an estimated uncertainty of 0.2 eV for the missing SESE contributions. Values are given in eV.

Correction	Numerical value
RMBPT	322.33(15)
Self energy	−55.87
SE screening	1.55
Vacuum polarization	12.94
VP screening	−0.39
SESE a) b) c)	uncalculated
SEVP a) b) c)	−0.19
S(VP)E	−0.02
VPVP a)	0.04
VPVP b)	0.03
VPVP c)	0.08
Two-photon reference state (box)	0.04
Two-photon reference state (cross)	−0.02
Recoil	−0.07
Nuclear polarization	0.03
Total theory	280.48(25)
Experiment	280.59(10)

3. g-factor calculations

The anomalous magnetic moment of the *free* electron is one of the most precise theoretically known quantities in physics. It is defined as

$$\frac{|\mu|}{\mu_{\mathrm{B}}} = g_S \frac{|S|}{\hbar}, \tag{10}$$

where

$$\mu_{\mathrm{B}} = \frac{e\hbar}{2m_{\mathrm{e}}} = 5.788\,382\,63(52) \times 10^{-11} \text{ MeV/T} \tag{11}$$

is the Bohr magneton [40] and g_S is the "g-factor" of the electron, which relates the magnetic moment to the spin of the electron. Relativistic Dirac theory predicts $g_S = 2$, and deviations from this value are known as the "anomalous magnetic moment of the electron spin". They are due to QED effects only, and their prediction and measurement have caused outstanding developments both in experimental and theoretical physics.

The experimental value of g_S for the free electron is known even better than the theoretical one (see [41,42], respectively):

$$g_S \text{ (expt.)} = 2\big(1 + 1\,159\,652\,188.4(4.3) \times 10^{-12}\big), \tag{12}$$

$$g_S \text{ (theo.)} = 2\big(1 + 1\,159\,652\,201\,(27) \times 10^{-12}\big). \tag{13}$$
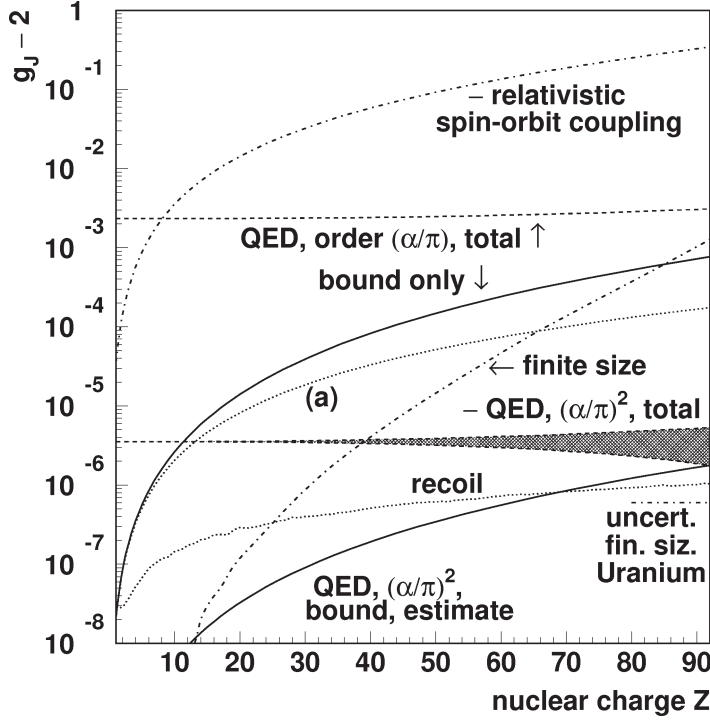
Figure 6. Contributions to the deviation of the g-factor of bound electrons from the value 2. The diagram is based on [51].

It should be mentioned, that (13) required the evaluation of 971 Feynman diagrams; 1, 7, 72 and 891 due to the first, second, third and fourth order in the power expansion of (α/π), respectively.

Only recently attempts were made to measure the g-factor of an electron in the very strong field of a heavy nucleus also [43]. Measurements exist up to now only for H and He [44–46]. However, the very promising test of a setup for measurements in much heavier ions also [10] forces theoreticians to consider seriously the calculations for the so-called bound-state g-factor as well. Several aspects have to be taken into account which do not exist for the g-factor of the free electron.

A summary of these effects is displayed by figure 6. We will discuss them separately in the following.

The relativistic spin-orbit coupling was derived by Breit [47] in 1928 already. It simply accounts for the fact that spin and angular momentum cannot be considered separately when a central potential is present. Therefore it is also not possible to measure the magnetic moment related to the spin of a bound electron separately. All g-factor measurements on bound electrons will probe the magnetic moment related to the *total* angular momentum J. We therefore always refer to the g-factor of bound electrons as g_J.
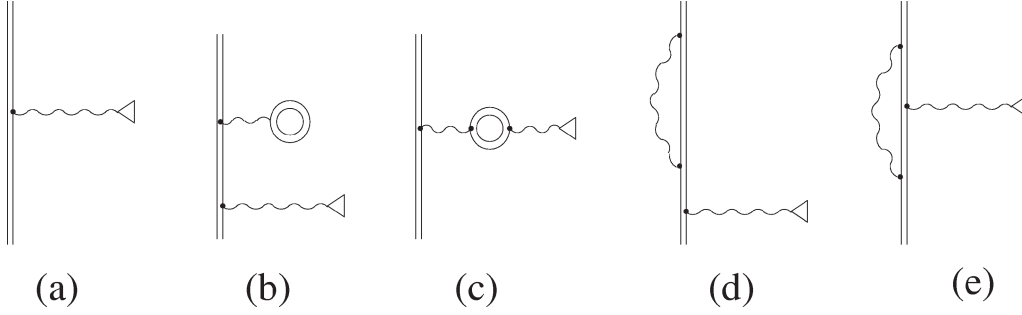
Figure 7. Feynman diagrams corresponding to the g-factor calculations for bound electrons. The triangle denotes interaction with an external magnetic field. Diagram (a) represents the basic interaction while diagrams (b)–(e) indicate the QED corrections of order (α/π).

The contribution due to spin-orbit coupling is known exactly and amounts to

$$\frac{4}{3}\left(\sqrt{1-(Z\alpha)^2}-1\right) \simeq -\frac{2}{3}(Z\alpha)^2 - \frac{1}{6}(Z\alpha)^4 - \frac{1}{9}(Z\alpha)^6 + \mathrm{O}\big((Z\alpha)^8\big) \qquad (14)$$

for the $1\mathrm{s}_{1/2}$ state, where we indicated the expansion in powers of $(Z\alpha)$ as well. Neglecting all QED and nuclear effects, the pure Dirac theory g_J-factor of an electron bound in the $1\mathrm{s}_{1/2}$ state can therefore be written as

$$g_{J\,\mathrm{Dirac}} = 2\left(\frac{2\sqrt{1-(Z\alpha)^2}+1}{3}\right). \qquad (15)$$

The diagram in figure 7(a) is the one corresponding to this simple interaction of a bound electron with an external magnetic field.

The Breit correction "relativistic spin-orbit coupling" and the QED correction of order $(\alpha/\pi)^2$ carry negative sign. The total QED corrections of first and second order in (α/π) (dashed lines) contain the contributions of the anomalous magnetic moment of the free electron as well as the corrections due to binding. These lines in the low-Z limit therefore indicate the coefficients of these contributions to g_S of the free electron. The corrections due to binding are displayed separately as well (solid lines). For the order $(\alpha/\pi)^2$ this contribution is given as an estimate only. The resulting uncertainty to the total QED contribution of this order is indicated by the hatched area. For the binding correction of order (α/π), also the first term of the $(Z\alpha)^2$ expansion is indicated (dotted line (a)).

For the recoil effect, (19) is displayed. Wiggles in the curve are due to the employed nuclear masses taken from [40].

Beneath the nuclear finite-size effect to the g-factor we also indicate its uncertainty for the particular case of ^{238}U. This value results from the uncertainty in the measured nuclear rms-radius.

All other corrections displayed in the diagram in figure 6 go beyond the point nucleus Dirac theory. We will discuss the QED corrections first. Commonly, these corrections are presented in the form

$$g_{J\,\text{QED}} = 2\left[\left(\frac{\alpha}{\pi}\right)C^{(2)}(Z\alpha) + \left(\frac{\alpha}{\pi}\right)^2 C^{(4)}(Z\alpha) + \cdots\right]. \qquad (16)$$

Here, the expansion in powers of (α/π) represents the expansion into Feynman diagrams with an according number of internal photon lines, similar to the Lamb shift. The functions $C^{(2i)}(Z\alpha)$ include the QED effects both for free electrons as well as for binding. An expansion into powers of $(Z\alpha)$ therefore yields the "free" contribution as the leading term. For example,

$$C^{(2)}(Z\alpha) = \frac{1}{2} + \frac{(Z\alpha)^2}{12} + \cdots. \qquad (17)$$

The leading term in this expansion is the famous quantum electrodynamical correction to the g-factor of the free electron which was obtained by Schwinger in 1948 [48]. The second term is the first correction which accounts for binding effects. It was derived by Grotch in 1970 [49]. However, as in the Lamb shift case it is clear that for heavy systems an expansion of the functions $C^{(2i)}$ into powers of $(Z\alpha)$ is not feasible at all. Recently, $C^{(2)}(Z\alpha)$ was calculated to all orders in $(Z\alpha)$ independently by two groups [50,51]. From the diagram in figure 6 it is evident that for uranium, the total contribution differs from the leading $(Z\alpha)^2$ term by almost one order of magnitude.

The techniques which were employed in calculating $C^{(2)}(Z\alpha)$ are very much the same as in Lamb shift calculations. In principle, the free fermion propagators have to be replaced by those for bound fermions, and then care has to be taken to renormalize and evaluate the diagrams properly. In particular, many techniques are the same as for hyperfine contribution calculations. For details we refer to the original works.

Unlike in the case of the Lamb shift, to our knowledge, *no* calculations for diagrams with more than one internal photon line have been carried out so far for the g-factor of bound electrons. The contribution from these diagrams in the free case, on the other hand, is analytically known to be

$$C^{(4)}(Z=0) = \frac{197}{144} + \left(\frac{1}{2} - 3\ln 2\right)\zeta(2) + \frac{3}{4}\zeta(3) \simeq -0.328\,478\,965\ldots \qquad (18)$$

for the $(\alpha/\pi)^2$ part.

To obtain an estimate for the magnitude of the binding effects, we simply multiplied the values obtained for the order (α/π) by another factor (α/π). This value is also indicated in figure 6. As it is an estimate only which could carry even the wrong sign, we both added and subtracted this term to $C^{(4)}(Z=0)$. The area between both curves is indicated in figure 6 as probable size of this yet unknown effect. It is noteworthy, that its expected size is by at least one order of magnitude larger than the indicated uncertainty due to the error in the determination of the radius of the uranium nucleus. The aimed experimental precision is expected to become even better, so that

binding effects in $C^{(4)}(Z\alpha)$ will be clearly visible and therefore should be calculated soon.

Contrary to this, the function $C^{(6)}(Z\alpha)$ is not expected to be of any importance at all. $C^{(6)}(Z = 0) = 1.181\,259(40)$, which results in a low-Z limit of about 2.9×10^{-8} in the total contribution to $g_J - 2$. Therefore we did not even indicate this value in figure 6.

Beneath the quantum electrodynamical effects, also nuclear properties contribute to the value of the g-factor. As it is the case for the Lamb shift and the hyperfine splitting, it is the insufficient knowledge of these properties which might hinder an exact theoretical prediction of the bound electron g-factor. However, this difficulty is less severe than in the other test fields, as we are going to point out now.

The values in (14) and (15) are those for a point-like nucleus which gives rise to an exact $1/r$ potential. Extended nuclei lead to a deviation from this potential which also implies wave functions different from the analytically known ones [14] for point-like nuclei. The numerical calculation of these wave functions to a suitable precision is not a difficulty nowadays, and the indicated finite-size correction to the spin-orbit coupling can therefore be considered as being well known, as it is the case for the "pure" size correction for the Lamb shift. Its uncertainty is due to the error in the nuclear radii which are utilized in the calculations. (As an example, we indicate the uncertainty of this effect for uranium.)

It should be mentioned, that nuclear size effects are included from the beginning in the numerical QED calculations to the order (α/π). Therefore, nuclear size effects to QED contributions are not listed here separately.

Next to nuclear size, the finite nuclear mass affects the g-factor in a way similar to the Lamb shift. Contrary to the latter, for the nuclear recoil contribution to the g-factor up to now only an expansion into powers of $(Z\alpha)$ is available, which was derived by Grotch and Hegstrom [52] in 1971. It yields

$$
g_{J\,\mathrm{recoil}} = (Z\alpha)^2 \left[\left(\frac{m_{\mathrm{e}}}{M_{\mathrm{N}}} \right) - (1 + Z) \left(\frac{m_{\mathrm{e}}}{M_{\mathrm{N}}} \right)^2 \right]
$$
$$
+ (Z\alpha)^2 \left(\frac{\alpha}{\pi} \right) \left[-\frac{1}{3} \left(\frac{m_{\mathrm{e}}}{M_{\mathrm{N}}} \right) + \frac{3 - 2Z}{6} \left(\frac{m_{\mathrm{e}}}{M_{\mathrm{N}}} \right)^2 \right]. \tag{19}
$$

We have grouped together terms according to the expansion into powers of (α/π) as well, and thus it is clear which are the corrections both to the purely relativistic spin-orbit coupling as well as to the QED effects. (19) is exact to orders $(Z\alpha)^2$, (α/π) and $(m_{\mathrm{e}}/M_{\mathrm{N}})^2$. Whereas the last two expansions are reasonable also for high-Z systems, the expansion into powers of $(Z\alpha)$ can be considered as approximation only, being even only an order-of-magnitude estimate for high-Z systems.

Not displayed in the diagram in figure 6 are the effects of internal nuclear degrees of freedom, which also could influence the g-factor via interactions like the one shown in figure 8. As in the Lamb shift case, these nuclear polarization contributions are thought to be of less than the magnitude of $(\alpha/\pi)^2$-QED effects, the more so, as
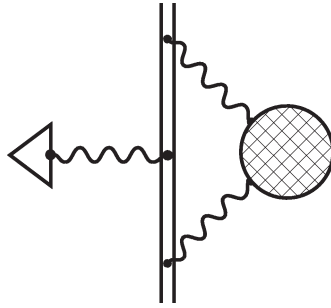
Figure 8. Feynman diagram for the nuclear polarization contribution to the g-factor.

nuclear effects tend to play only a minor role for the g-factor. These yet unknown effects therefore are not thought to influence the g-factor at the aimed precision of measurement, and therefore there seems to be no principal limit from the theoretical side to calculate the g-factor of the bound electron to an accuracy to 10^{-7}, although this work has by far not yet been completed.

4.   Conclusion

We investigated various contributions to the Lamb shift in heavy highly charged ions and to the g-factor of bound electrons. The major contributions to both effects are well known. Also higher order QED contributions seem to be calculable in principle, although this work has not yet been completed. On the same level of precision, different contributions come into play which are mainly caused by effects of non-QED origin, such as nuclear polarization. Some of these, as Z_0-boson exchange or boundary effects seem to be negligible, some are well to handle, e.g., nuclear recoil. Especially for contributions caused by the nucleus, experimental data enter the calculations which are not known with sufficient accuracy. Furthermore, the size of these effects is similar to that of higher-order QED effects so that the experimental probe of QED in strong fields is therefore inherently limited. From our discussion of both effects it is evident, that especially g-factor measurements in the high-Z region could test more clearly QED effects of order $(\alpha/\pi)^2$ than it might be possible with the Lamb shift.

Acknowledgements

References

[1] G. Soff, T. Beier and C. Hofmann, Acta Phys. Polon. B 27 (1996) 369.

[2] T. Stöhlker, P.H. Mokler, K. Beckert, F. Bosch, H. Eickhoff, B. Franzke, M. Jung, T. Kandler, O. Klepper, C. Kozhuharov, R. Moshammer, F. Nolden, H. Reich, P. Rymuza, P. Spädtke and M. Steck, Phys. Rev. Lett. 71 (1993) 2184.

[3] H.F. Beyer, D. Liesen, F. Bosch, K.D. Finlayson, M. Jung, O. Kleppner, R. Moshammer, K. Beckert, H. Eickhoff, B. Franzke, F. Nolden, P. Spädtker, M. Steck, G. Menzel and R.D. Deslattes, Phys. Lett. A 184 (1994) 435.

[4] H.F. Beyer, IEEE Trans. Instrum. Meas. 44 (1995) 510.
H.F. Beyer, G. Menzel, D. Liesen, A. Gallus, F. Bosch, R. Deslattes, P. Indelicato, Th. Stöhlker, O. Klepper, R. Moshammer, F. Nolden, H. Eickhoff, B. Franzke and M. Steck, Z. Phys. D 35 (1995) 169.

[5] J. Schweppe, A. Belkacem, L. Blumenfeld, N. Claytor, B. Feinberg, H. Gould, V.E. Costram, L. Levy, S. Misawa, J.R. Mowat and M.H. Prior, Phys. Rev. Lett. 66 (1991) 1434.

[6] I. Klaft, S. Borneis, T. Engel, B. Fricke, R. Grieser, G. Huber, T. Kühl, D. Marx, R. Neumann, S. Schröder, P. Seelig and L. Völker, Phys. Rev. Lett. 73 (1994) 2425.

[7] J.R. Crespo Lopez-Urrutia, P. Beiersdorfer, D. Savin and K. Widman, Phys. Rev. Lett. 77 (1996) 826.

[8] P. Seelig, S. Borneis, A. Dax, T. Engel, S. Faber, M. Gerlach, C. Holbrow, G. Huber, T. Kühl, D. Marx, K. Meier, P. Merz, W. Quint, F. Schmitt, L. Völker, H. Winter, M. Würtz, K. Beckert, B. Franzke, F. Nolden, H. Reich and M. Steck, this issue.

[9] P. Beiersdorfer, A. Osterheld, J. Scofield, J.R. Crespo Lopez-Urrutia and K. Widmann, Lawrence Livermore National Laboratory Report UCRL-JC-127437 (1997) p. 18.

[10] W. Quint et al., this issue.

[11] V.M. Shabaev, M.B. Shabaeva, I.I. Tupitsyn and V.A. Yerokhin, this issue.

[12] W.E. Lamb, Jr. and R.C. Retherford, Phys. Rev. 72 (1947) 241.

[13] G. Soff, T. Beier, M. Greiner, H. Persson and G. Plunien, Advances in Quantum Chemistry 30 (1998) 125.

[14] M.E. Rose, *Relativistic Electron Theory* (Wiley, New York, 1961).

[15] P.J. Mohr, Ann. Physics (NY) 88 (1974) 26;
P.J. Mohr, Ann. Physics (NY) 88 (1974) 52;
P. Indelicato and P.J. Mohr, Phys. Rev. A 46 (1992) 172;
P.J. Mohr, Physica Scripta 46 (1993) 44.

[16] H.M. Quiney and I.P. Grant, Physica Scripta 46 (1993) 132;
H.M. Quiney and I.P. Grant, J. Phys. B 27 (1994) L299;
H. Persson, I. Lindgren and S. Salomonson, Physica Scripta 46 (1993) 125;
I. Lindgren, H. Persson, S. Salomonson and A. Ynnerman, Phys. Rev. A 47 (1993) R4555.

[17] H. Persson, I. Lindgren, L. Labzowsky, T. Beier, G. Plunien and G. Soff, Phys. Rev. A 54 (1996) 2805.

[18] I. Lindgren, H. Persson, S. Salomonson and P. Sunnergren, Evaluation of two-loop electron self energies for tightly bound electrons, Preprint, Department of Physics, Chalmers University of Technology and Göteborg University, Sweden.

[19] S. Mallampalli and J. Sapirstein, Fourth-order self-energy contribution to the Lamb shift, Preprint, Department of Physics, University of Notre Dame, Notre Dame, IN, USA.

[20] L. Labzowsky and A. Mitrushenkov, Phys. Lett. A 198 (1995) 333;
A. Mitrushenkov, L. Labzowsky, I. Lindgren, H. Persson and S. Salomonson, Phys. Lett. A 200 (1995) 51;
L.N. Labzowsky and A.O. Mitrushenkov, Phys. Rev. A 53 (1996) 3029;
L.N. Labzowsky and I.A. Goidenko, J. Phys. B 30 (1997) 177.

[21] G. Plunien, T. Beier, G. Soff and H. Persson, European Physical Journal D 1 (1998) 177.

[22] S. Mallampalli and J. Sapirstein, Phys. Rev. A 54 (1996) 2714.

[23] H. Persson, I. Lindgren, S. Salomonson and P. Sunnergren, Phys. Rev. A 48 (1993) 2772.

[24] T. Beier, G. Plunien, M. Greiner and G. Soff, J. Phys. B 30 (1997) 2761.

[25] T. Beier and G. Soff, Z. Phys. D 8 (1988) 129.

[26] S.M. Schneider, W. Greiner and G. Soff, J. Phys. B 26 (1993) L529.

[27] I. Lindgren, H. Persson, S. Salomonson, V. Karasiev, L. Labzowsky, A. Mitrushenkov and M. Tokman, J. Phys. B 26 (1993) L 503.

[28] A.N. Artemyev, V.M. Shabaev and V.A. Yerokhin, Phys. Rev. A 52 (1995) 1884.

[29] A.N. Artemyev, V.M. Shabaev and V.A. Yerokhin, J. Phys. B 28 (1995) 5201.

[30] V.M. Shabaev, J. Phys. B 26 (1993) 1103.

[31] G. Fricke, C. Bernhardt, K. Heilig, L.A. Schaller, L. Schellenberg, E.B. Shera and C.W. de Jager, At. Data and Nucl. Data Tables 60 (1995) 177.

[32] J.D. Zumbro, E.B. Shera, Y. Tanaka, C.E. Bemis Jr., R.A. Naumann, M.V. Hoehn, W. Reuter and R.M. Steffen, Phys. Rev. Lett. 53 (1984) 1888.

[33] P.J. Mohr and G. Soff, Phys. Rev. Lett. 70 (1993) 158.

[34] W.R. Johnson and G. Soff, At. Data and Nucl. Data Tables 33 (1985) 405.

[35] J.D. Zumbro, R.A. Naumann, M.V. Hoehn, W. Reuter, E.B. Shera, C.E. Bemis, Jr. and Y. Tanaka, Phys. Lett. 167 B (1986) 383.

[36] G. Plunien, B. Müller, W. Greiner and G. Soff, Phys. Rev. A 43 (1991) 5853;
G. Plunien and G. Soff, Phys. Rev. A 51 (1995) 1119; Phys. Rev. A 53 (1996) 4614.

[37] I. Bednyakov, L. Labzowsky and G. Soff, J. Phys. B 28 (1995) L719.

[38] H.B.G. Casimir, Proc. Kon. Ned. Akad. Wet. 51 (1948) 793.

[39] G. Plunien, B. Müller and W. Greiner, Phys. Rep. 134 (1986) 87.

[40] Review of particle properties, Phys Rev. D 50 (1994) 1173.

[41] R.S. Van Dyck, Jr., P.B. Schwinberg and H.G. Dehmelt, Phys. Rev. Lett. 59 (1987) 26.

[42] T. Kinoshita, Phys. Rev. Lett. 75 (1995) 4728.

[43] K. Hermanspahn, W. Quint, S. Stahl, M. Tönges, G. Bollen, H.-J. Kluge, R. Ley, R. Mann and G. Werth, Acta Phys. Polon. B 27 (1996) 357.

[44] F.G. Walther, W.D. Philips and D. Kleppner, Phys. Rev. Lett. 28 (1972) 1159.

[45] J.S. Tiedeman and H.G. Robinson, Phys. Rev. Lett. 39 (1977) 602.

[46] C.E. Johnson and H.G. Robinson, Phys. Rev. Lett. 45 (1980) 250.

[47] G. Breit, Nature 122 (1928) 649.

[48] J. Schwinger, Phys. Rev. 73 (1948) 416.

[49] H. Grotch, Phys. Rev. Lett. 24 (1970) 39.

[50] S.A. Blundell, K.T. Cheng and J. Sapirstein, Phys. Rev. A 55 (1997) 1857.

[51] H. Persson, S. Salomonson, P. Sunnergren and I. Lindgren, Phys. Rev. A 56 (1997) R2499.

[52] H. Grotch and R.A. Hegstrom, Phys. Rev. A 4 (1971) 59.